

# Reverse-time demigration using the extended-imaging condition

Wiktor Waldemar Weibull<sup>1</sup> and Børge Arntsen<sup>1</sup>

## ABSTRACT

The forward and inverse process of seismic migration and demigration or remodeling has many useful applications in seismic data processing. We evaluated a method to reobtain the seismic reflection data after migration, by inverting the common image point gathers produced by reverse-time migration (RTM) with an extended-imaging condition. This provided a transformation of the results of seismic data processing in the image domain back to the data domain. To be able to reconstruct the data with high fidelity, we set up demigration as a least-squares inverse problem and we solved it iteratively using a steepest-descent method. Because we used an extended-imaging condition, the method is not dependent on an accurate estimate of the migration-velocity field, and it is able to accurately reconstruct both primaries and multiples. At the same time, because the method is based on RTM, it can accurately handle seismic reflection data acquired over complex geologic media. Numerical results showed the feasibility of the method and highlighted some of its applications on 2D synthetic and field data sets.

## INTRODUCTION

The motivation behind this work was to obtain a method to reconstruct seismic reflection data from common image point gathers (CIGs) constructed with reverse time migration (RTM). The method should work without the need for an accurate velocity model, and the reconstructed data should have an acceptably small error in amplitude and phase. This would ultimately allow us to process data in the migrated domain, which can be an advantage in the case of seismic data acquired over complex geologic media.

Most classical seismic data processing methods in the data domain are based on simplified assumptions about the subsurface

structure, such as horizontal layering and mild lateral variations in mechanical properties. Over such media, reflection data can be described by simple equations such as hyperbolas. However, complex geologic media will cause complicated waveforms as seismic waves propagate through them. As the medium deviates from the simple models, the complexity of the reflection data increases and the classical seismic data processing methods start to fail. This calls for special treatment of complex data, which substantially complicates seismic data processing. On the other hand, the image domain allows unified treatment of data acquired over simple and complex media because the effects of the medium on the kinematics of wave propagation are largely removed by the process of back propagation, which is inherent to the migration procedure. This characteristic makes the image domain a powerful alternative to the data domain for seismic data processing. A challenge in designing seismic data processing methods in the image domain is the need for an accurate estimate of the migration velocities. In this work, we show how we can relax this requirement. We also show how we can, through demigration, transform the results of seismic data processing in the image domain back to the data domain.

Demigration methods have a long history in seismic data processing. [Loewenthal et al. \(1976\)](#) introduce the concept of the exploding reflector model, showing how to obtain zero-offset seismic data from a migrated stack using a background velocity model and wave theoretical methods. The Kirchhoff integral and the high-frequency approximation have also been used for reconstruction of seismic data from migrated images ([Jaramillo and Bleistein, 1999](#); [Santos et al., 2000](#); [Miranda, 2006](#)). More recently, RTM has been used to recreate data from seismic images with the purpose of velocity analysis ([Chauris and Benjemma, 2010](#)) and multiple attenuation ([Zhang and Duan, 2012](#)).

In their work, [Chauris and Benjemma \(2010\)](#) use the concept of the extended imaging condition ([Sava and Vasconcelos, 2011](#)) in a migration/demigration scheme. The advantage of the extended imaging condition over the classical crosscorrelation imaging condition ([Claerbout, 1971](#)), is that it preserves the phase and angle dependent amplitude information of the data in the migrated image, even in the case of migration with an inaccurate velocity model.

Manuscript received by the Editor 24 June 2013; revised manuscript received 12 November 2013; published online 22 May 2014.

<sup>1</sup>Norwegian University of Science and Technology, Institute for Petroleum Technology and Applied Geophysics, Trondheim, Norway. E-mail: wiktor.weibull@ntnu.no; borge.arntsen@ntnu.no.

© 2014 Society of Exploration Geophysicists. All rights reserved.

This is because when there are significant inaccuracies in the velocity model, or the data are contaminated by multiple reflections, a substantial amount of reflection energy is mapped outside of the zero-lag crosscorrelation during imaging. All reflection energy can be preserved in the image if the imaging condition is extended to a lagged crosscorrelation (Sava and Vasconcelos, 2011). Thus, when the reflection data are contaminated by the presence of multiple scattering, and when the migration velocity is inaccurate, the extended image has the potential to allow better linearized remodeling of the reflection data than a nonextended reflectivity model (Symes, 2008). Here, we explore this fact and use extended images to set up a demigration method in which we reconstruct the prestack seismic reflection data from the migrated image by minimizing a least-squares function.

The method we present is intimately related to the least-squares migration (LSM) method (Nemeth et al., 1999), if we note that LSM can also be formulated using extended images. The main difference between LSM and the proposed demigration procedure is in the organization of the inversion. Whereas the aim of LSM is to obtain an optimal reflectivity model of the subsurface, the aim of our method is to optimally remodel the data from the migrated image, in particular after some processing has been applied to it. This means that in LSM, remodeling is carried out using a Born forward modeling operator, whereas the image is obtained by solving a linear least-squares inverse problem, which aims at minimizing the difference between the observed data and the data remodeled from the image. On the other hand, in the proposed demigration, the migration step is done using the adjoint of a Born forward modeling operator (Claerbout, 1992), whereas the remodeling is carried out by solving a linear least-squares inverse problem, to be described later. In this regard, the proposed method is exactly the converse of LSM.

Numerical experiments show that our demigration procedure is robust and fast, in the sense that it does not require many iterations to adequately remodel the data, even when using a simple optimization scheme such as the steepest-descent method, and a relatively inaccurate migration velocity model. The 2D synthetic and field data examples highlight some applications of demigration, such as data interpolation and multiple attenuation.

## METHOD

The main purpose of the method is to be able to reconstruct seismic data from modified CIGs constructed using RTM with an extended imaging condition (Sava and Vasconcelos, 2011). In the extended imaging condition, instead of the classical crosscorrelation of the source and receiver wavefields at the imaging point (Claerbout, 1971), CIGs are constructed by crosscorrelating the source and receiver wavefields at symmetric lags around the imaging point. These crosscorrelation lags can be either spatial (Rickett and Sava, 2002) or temporal lags (Sava and Fomel, 2006). The important point is that, different from the classical imaging condition, the extended imaging condition preserves the kinematic and angle-dependent information of the data in the image, even in the case of migration with an inaccurate velocity model. This property is of fundamental importance because, in practice, the data are never single scattering, and the migration velocity model can never be known exactly.

In principle, any prestack image gather, such as the shot or angle gathers, can be used to reconstruct the prestack seismic reflection data. Here, we show how we can use the extended imaging

condition to set up a demigration method. We demonstrate the method using a time-domain implementation of RTM with a space-lag crosscorrelation imaging condition (Rickett and Sava, 2002):

$$\mathcal{R}^0(\mathbf{x}, \mathbf{h}) = \int ds \int dt W_s(\mathbf{x} - \mathbf{h}, t, s) \int d\mathbf{x}' \times \int dt' G(\mathbf{x} + \mathbf{h}, t; \mathbf{x}', t') P^0(\mathbf{x}', T - t', s), \quad (1)$$

where  $\mathcal{R}^0$  are CIGs (extended image),  $\mathbf{x} = (x, y, z)$  are the spatial coordinates,  $\mathbf{h} = (h_x, h_y, h_z)$  are half spatial lags,  $t$  is the time,  $T$  is the final recording time,  $s$  is the source index,  $W_s$  are source wavefields,  $G$  is the acoustic Green's function, and  $P^0(\mathbf{x}', t', s)$  are common shot gathers. Note that the summation over  $t'$  is equivalent to a time convolution and that the data used in migration is time reversed.

The source wavefields are given by

$$W_s(\mathbf{x}, t, s) = \int d\mathbf{x}' \int dt' G(\mathbf{x}, t; \mathbf{x}', t') S(\mathbf{x}', t', s), \quad (2)$$

where  $S$  are source functions.

Although here we develop the theory using a complete set of half spatial lags ( $h_x, h_y$ , and  $h_z$ ), in most cases it is sufficient to only use a subset of these. For the numerical examples contained in this paper, we only use the horizontal spatial lags, which are most sensitive to waves propagating at near-vertical angles. However, in cases where significant reflection energy turns horizontal, it might be important to incorporate the vertical spatial lags ( $h_z$ ) (Biondi and Shan, 2002).

Assume now that we have the CIGs ( $\mathcal{R}^0$ ) and we would like to obtain the data ( $P^0$ ); that is, we are interested in the inverse procedure of equation 1. One approach is to apply the adjoint of migration, which, for the extended imaging condition, can be written as (Weibull and Arntsen, 2013)

$$P(\mathbf{x}, t, s) = \int d\mathbf{x}' \int dt' G(\mathbf{x}, t; \mathbf{x}', t') \int d\mathbf{h} \frac{\partial^2 \mathcal{R}^0}{\partial z^2}(\mathbf{x}' - \mathbf{h}, \mathbf{h}) \times W_s(\mathbf{x}' - 2\mathbf{h}, t', s). \quad (3)$$

This equation is successfully used by Weibull and Arntsen (2013) to reconstruct seismic data from muted CIGs. A similar equation is used by Chauris and Benjema (2010) for velocity analysis. One problem with this modeling equation is that, even if it properly recreates the kinematics, it gives the wrong amplitudes for the data. Another approach, as proposed by this paper, is to cast the problem as a least-squares inversion of the following objective function:

$$\mathcal{J} = \frac{1}{2} \int d\mathbf{x} \int d\mathbf{h} \left\{ \frac{\partial}{\partial z} [\mathcal{F} \mathcal{R}^0(\mathbf{x}, \mathbf{h})] - \frac{\partial \mathcal{R}}{\partial z}(\mathbf{x}, \mathbf{h}) \right\}^2, \quad (4)$$

where  $\mathcal{R}^0$  is the extended image CIGs that are migrated from the observed shot gathers  $P^0$  using RTM;  $\mathcal{R}$  is the forward mapped CIGs, computed using the same equation (equation 1) and the same source wavefields  $W_s$ , but with the unknown/predicted shot gathers  $P$ ; and  $\mathcal{F}$  is an operator, such as muting or filtering that modifies  $\mathcal{R}^0$  prior to demigration. The vertical spatial derivatives in equation 4

are used to remove well-known artifacts from RTM images (Guitton et al., 2007).

By minimizing this objective function (equation 4), we seek to find the data that, when migrated and first-order derived in the  $z$ -direction, will approximate the image  $\frac{\partial}{\partial z}(\mathcal{F}\mathcal{R}^0)$  in a least-squares sense. In principle, because of the linear relationship between the data and the receiver wavefields, the problem is linear and its solution can be sought explicitly. The problem is that the data we are trying to estimate consist of  $N_s N_r N_t$  parameters, where  $N_s$  is the number of sources,  $N_r$  is the number of receivers, and  $N_t$  is the number of time samples. Due to the large number of parameters, we deem an explicit solution to be too computationally expensive. For the same reason, we also avoid methods based on an iterative solution of the normal equations. Instead, here we choose to solve the proposed least-squares problem using an out-of-core implementation of the steepest-descent method (Nocedal and Wright, 2000). The out-of-core solution means that all optimization operations are carried out on disk. This removes the need to store the parameter vector in memory, and it allows optimization of data sets of virtually any size. In the steepest-descent method, the demigrated shot gathers are updated iteratively according to

$$P_{i+1}(\mathbf{x}, t, s) = P_i(\mathbf{x}, t, s) - \alpha_i \frac{\partial \mathcal{J}}{\partial P_i}(\mathbf{x}, t, s), \quad (5)$$

where  $i \in (1, \dots, N)$  is the iteration index,  $\alpha_i$  is a positive step length, and  $\partial \mathcal{J} / \partial P_i$  is given by

$$\frac{\partial \mathcal{J}}{\partial P_i}(\mathbf{x}, t, s) = \int d\mathbf{x}' \int dt' G(\mathbf{x}, t; \mathbf{x}', t') \int d\mathbf{h} \frac{\partial^2 \Delta \mathcal{R}_i}{\partial z^2}(\mathbf{x}' - \mathbf{h}, \mathbf{h}) \times W_s(\mathbf{x}' - 2\mathbf{h}, t', s), \quad (6)$$

with the image residual  $\Delta \mathcal{R}_i$  being given by

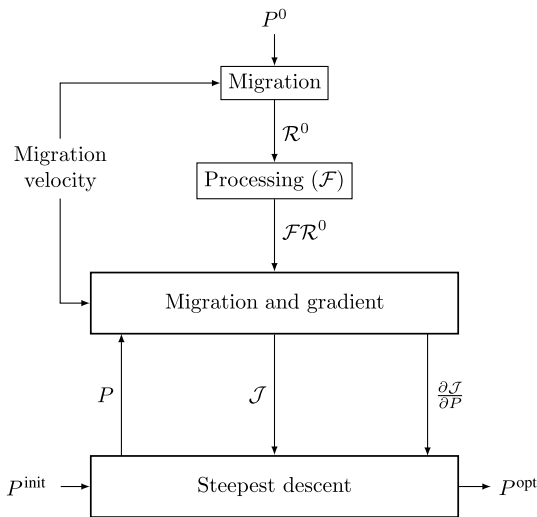


Figure 1. Demigration organization flowchart. In this diagram,  $P^0$  represents the original data,  $P^{\text{init}}$  are the initial data, and  $P^{\text{opt}}$  are the optimal reconstructed data.

$$\begin{aligned} \Delta \mathcal{R}_i(\mathbf{x}, \mathbf{h}) &= \mathcal{F}\mathcal{R}^0(\mathbf{x}, \mathbf{h}) - \int ds \int dt W_s(\mathbf{x} - \mathbf{h}, t, s) \\ &\times \int d\mathbf{x}' \int dt' G(\mathbf{x} + \mathbf{h}, t; \mathbf{x}', t') \\ &\times P_i(\mathbf{x}', t', s). \end{aligned} \quad (7)$$

In deriving equation 6, we used the fact that  $\int dz \frac{\partial \mathcal{R}}{\partial z} \frac{\partial \mathcal{R}}{\partial z} \approx -\int dz \frac{\partial^2 \mathcal{R}}{\partial z^2} \mathcal{R}$ . This explains the origin of the second-order vertical derivatives. The necessary boundary conditions for computing the gradient  $(\partial \mathcal{J} / \partial P_i)$  are the same as those used in migration; that is, the quantities to the right of the Green's functions are inserted as sources in the solution of the acoustic wave equation. Absorbing boundary conditions are used to avoid reflections from the boundaries of the numerical grids. Finally, we assume an initial state of rest, with  $\frac{\partial \mathcal{J}}{\partial P_i}(\mathbf{x}, 0, s) = 0$  at time zero.

The organization of the demigration algorithm is shown in Figure 1. First, the original reflection data  $P^0$  are migrated using equation 1 and are subject to an arbitrary processing operation represented by the operator  $\mathcal{F}$ . The data are then reconstructed iteratively using the steepest-descent algorithm. The optimization requires an initial estimate of the data ( $P^{\text{init}}$ ). In practice, the initial data can be the original data or zero. In the case that the original data are used (our example 3), the effects of processing in the image domain will be iteratively transferred to the original data. This is the best option if the phase and amplitude characteristics of the original data are to be optimally preserved. Another option is to fully rely on the migrated image  $(\mathcal{F}\mathcal{R}^0)$  to estimate the data; in this case, the initial data are set to zeros with the desired geometry information (our examples 1 and 2). This option can be useful if the demigration is to be used to simulate a different geometry than the original data, such as in illumination studies or in data interpolation. Independent of the choice of the initial data, at each iteration of steepest descent, a migration and a gradient computation must be performed. These procedures are performed using equations 1 and 6, respectively. The source-side wavefields  $W_s$  are computed only once and stored on disk because they are independent of the data, and the migration velocities are the same as those used to migrate the original data. Once the objective function is evaluated and the gradient is computed, the data  $P$  can be updated according to equation 5, where the step length  $\alpha$  is computed using a line-search method (Nocedal and Wright, 2000). After a predetermined number of iterations has been run, or if the objective function error is small enough, the reconstructed data  $P^{\text{opt}}$  are returned.

## NUMERICAL EXAMPLES

We illustrate the method with some 2D seismic examples. The first two examples are based on the Marmousi model (Versteeg, 1993), which has become a benchmark model for complex geology. This model, shown in Figure 2, is used to generate seismic data using a finite-difference modeling code (Virieux, 1986). We use a monopole point source and Ricker wavelet with dominant frequency of 20 Hz. We use absorbing boundary conditions on all sides to simulate data without free-surface-related multiples. The source spacing and the receiver spacing are both 0.025 km. The shot gathers have a minimum offset of 0 km and a maximum offset of 5 km.

In the last example, we explore the application of demigration to field data. The data consist of a 2D marine seismic line acquired

over the Norwegian North Sea. There are 460 shot gathers, each with a minimum offset of 0.075 km and a maximum offset of 1.25 km. The source and receiver spacing is 0.0125 km. The dominant frequency of the data is  $\approx 30$  Hz, and the maximum frequency is  $\approx 80$  Hz.

### Example 1

In the first example, we show the ability of the method to reconstruct the seismic prestack data from stacked migrated CIGs. In this procedure, the CIGs that are input for demigration are the CIGs that are output from RTM with the original data, without any processing applied to it.

The purpose is to illustrate the ability of the method to reconstruct the seismic data from the migrated CIGs, even in the case that the migration velocity model has significant errors.

The migration velocity model, shown in Figure 3, is a strongly smoothed version of the true velocity model. We discretized the migration velocity model using a grid cell size of  $0.0125 \times 0.0125$  km in the  $x$ - and  $z$ -directions, and we use it for the forward- and reverse-time modeling steps needed for migration. The maximum time used in modeling is 4 s. The time-step size is limited by numerical stability criteria (Virieux, 1986) and is chosen to be 0.8 ms, but the wavefields needed for the imaging condition are sampled every 4 ms. As the source functions, we use monopole point sources with a 20-Hz dominant frequency Ricker wavelet.

The amount of lag used in the extended imaging condition is a very important parameter for the proposed demigration method.

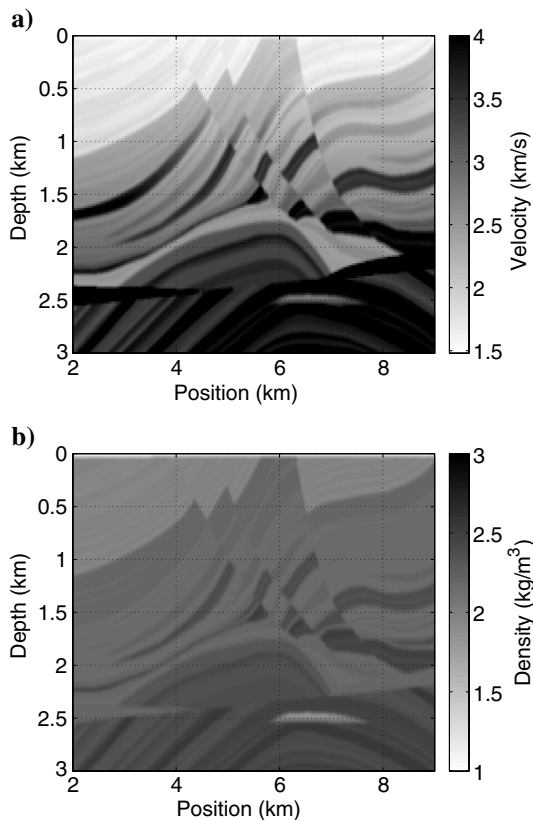


Figure 2. Marmousi acoustic model. (a) Velocity model. (b) Density model.

Ideally, the size of the half-offset vector must be chosen such that most, if not all, of the energy is contained in the image. Otherwise, important information might not be available for demigration and will thus lead to some loss of reflection data. The choice of the number of subsurface offset lags needed in the crosscorrelation depends on the accuracy of the migration velocity model. The farther the model is from the correct model, the farther away from zero lag will the energy be migrated into, and the larger the half-offset vector needs to be. Another important consideration is whether the data are single scattering or if they contain multiple reflections. Due to the linear model inherent to migration (single scattering Born approximation), all events in the data, including multiples, are treated as if they were primary reflections. Because primaries and multiples have conflicting moveouts (free-surface-related multiples generally require lower migration velocities to focus), even for accurate migration velocities (for primaries), significant multiple energy will be mapped to nonzero half-offset lags (Mulder and van Leeuwen, 2008). To preserve this multiple energy, it is therefore necessary to have the proper amount of lag in the extended imaging condition.

The half-offset sampling interval is the same as the spatial sampling interval of the wavefields. In this example, we use 251 horizontal half-offset lags in the crosscorrelation, which produces a half-offset vector ranging between  $-1.56$  and  $1.56$  km. Aliasing effects due to coarse sampling of the half-offset vector are not considered in the current study. However, in the case that aliasing effects turn to be a problem, the sampling interval can be halved by only shifting one of the wavefields in the imaging condition (Rickett and Sava, 2002).

The migrated stacked image (zero-lag) and a collection of CIGs are shown in Figure 4. As expected, because the migration velocity model is nonoptimal, the zero-lag image is not well focused, and significant energy is spread out over the subsurface nonzero half-offset lags. Yet, most energy is preserved within the center of the CIGs, tapering off toward the edges. This implies that the choice of 251 half-offset lags is large enough as to preserve the reflection energy from the data into the migrated image.

In demigration, the initial shot gathers are a collection of zeroed traces. This means that we fully rely on the CIGs to reconstruct the reflection data. Figure 5 shows a comparison of a particular shot gather at source position 7.83 km of the original data with the result of demigration of the CIGs after one iteration and after nine iterations of demigration. In this comparison, the reconstructed shot gathers were scaled by an optimal scalar constant. This constant

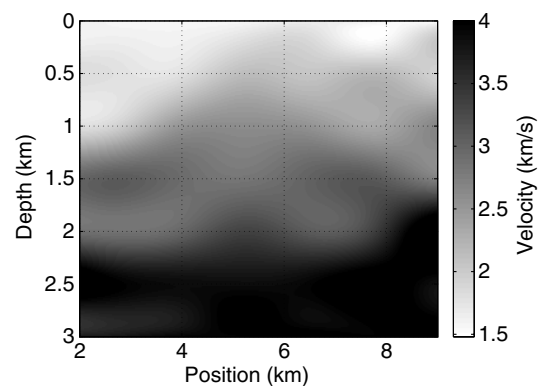


Figure 3. Marmousi migration velocity model used in example 1.

was found by minimizing the least-squares difference of the amplitudes between the reconstructed shot gathers and the original shot gathers. Figure 5d shows the difference between the original shot gather and the reconstructed shot gather of Figure 5c. As the figure shows, there are some differences between the reconstructed shot gather and the original shot gather. These differences seem to be located in the low and high ends of the temporal frequency spectrum (see also Figure 6), and they might decrease by running more iterations of steepest descent. However, after nine iterations, the change in the objective function with iterations is very small. It is possible that a better result can be achieved by using a more efficient optimization algorithm, such as the conjugate gradient method or the limited-memory Broyden–Fletcher–Goldfarb–Shanno algorithm (L-BFGS) method (Nocedal and Wright, 2000), or by including a preconditioner.

Figure 6 shows a comparison of traces from the original data and from the demigrated data after one iteration and after nine iterations of demigration. The results show that the kinematics of the data are well reconstructed already after one iteration, and after nine iterations, the data amplitudes are getting closer to the ones in the original data, as can be seen in the comparison of the time traces (Figure 6a–6c), as well as in the comparison of the amplitude spectra (Figure 6d).

For comparison, we repeat the above example, but this time using only the zero-lag image; that is, we are interested in comparing the results of using an extended imaging condition against those obtained when only using the classical crosscorrelation imaging condition. Figure 7a and 7b shows, respectively, the original shot gather at position 6.33 km and a shot gather at the same position, but obtained by demigration of the zero-lag image. For comparison, Figure 7c shows the result of demigration using the extended image. Both demigrated gathers correspond to the results of demigration after nine iterations. The figure clearly shows that, due to the errors in the velocity model, demigration of the zero-lag image is unable to fully reconstruct the kinematics of the data. The main reason for this is because the velocity model is inaccurate, significant energy is migrated out of the zero lag and is made unavailable for demigration.

## Example 2

In the second example, we explore the application of demigration to interpolation of data. The ability of demigration to interpolate reflection seismic data comes from the fact that, in the process of migration and demigration, the Huygens-Fresnel principle is applied two times: once during extrapolation from the receivers to the image points and another time during extrapolation from the image points back to the receivers. In addition, in migration, redundant information contained in the reflection data is gathered at the imaging points and can be used to fill in gaps left by incomplete seismic data acquisition. A similar type of data reconstruction is presented by Nemetz et al. (1999) in the context of LSM.

To illustrate the application of demigration to data interpolation, the Marmousi data of the previous example are decimated by only taking every eighth receiver. The resulting receiver

interval of 0.2 km introduces severe dip aliasing in the seismic data recording (Figure 8). For reasons that will become clear later, we use a more accurate migration velocity model to migrate the data in this example. The migration velocity model used is shown in Figure 9. The model is obtained through wave-equation-migration

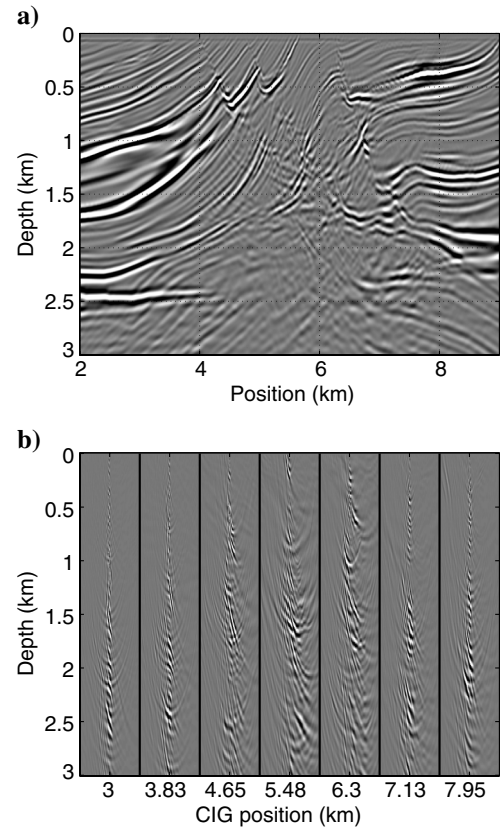


Figure 4. Marmousi migrated (a) zero-lag image and (b) CIGs at several selected spatial positions. In the CIGs, the half-offsets range between  $-1.56$  and  $1.56$  km.

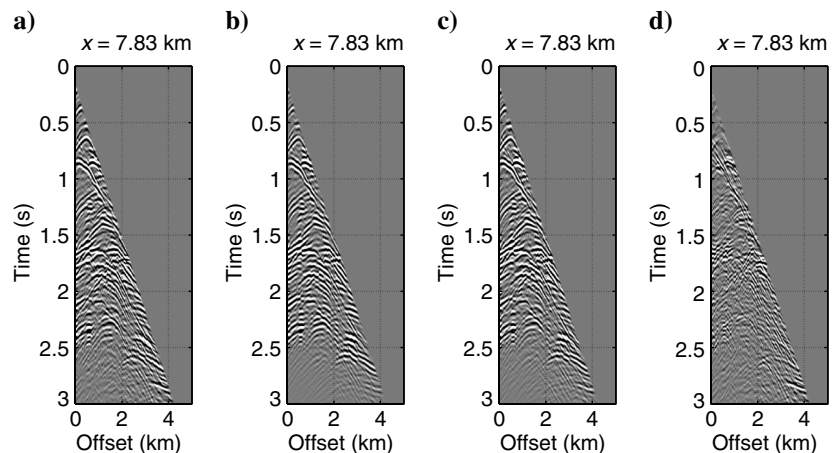


Figure 5. Marmousi shot gathers at source position 7.83 km; (a) original, (b) reconstructed after one iteration of demigration, (c) reconstructed after nine iterations of demigration, and (d) difference between shot gathers (a and c).

velocity analysis (Weibull and Arntsen, 2013), using the model in Figure 3 as a starting model. In building the CIGs, we use 121 horizontal half spatial lags in the imaging condition, which gives a half-offset vector ranging between  $-0.75$  and  $0.75$  km.

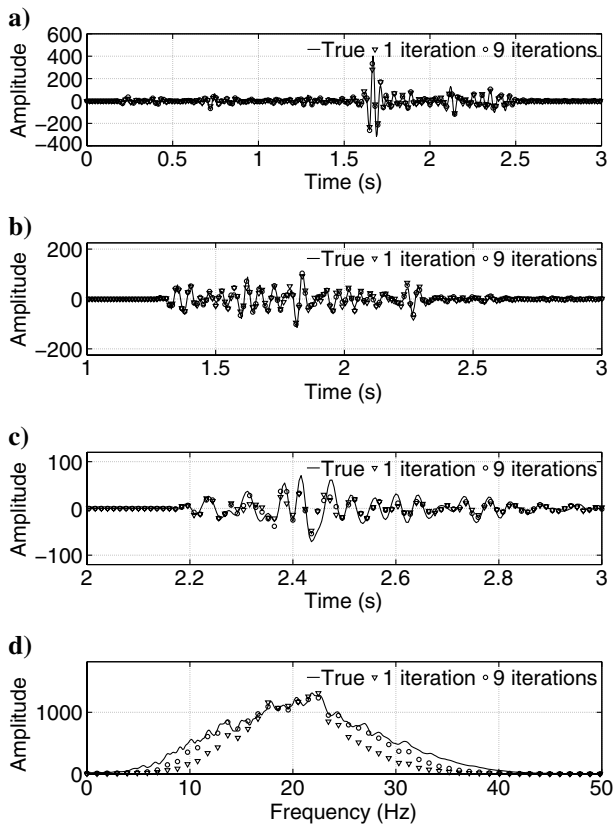


Figure 6. Comparison of traces of the Marmousi shot gather at source position 7.83 km; (a) at zero offset, (b) at 1.65-km offset, and (c) at 3-km offset. (d) Comparison of amplitude spectra averaged over all traces of the shot gather.

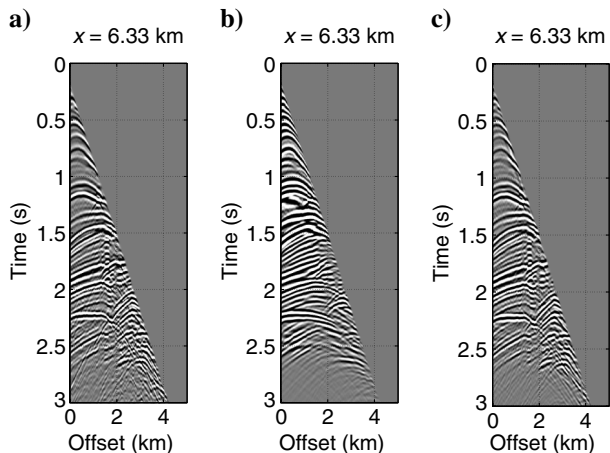


Figure 7. Marmousi shot gathers at source position 6.33 km; (a) original, (b) reconstructed from the zero-lag image after nine iterations of demigration, (c) reconstructed from the extended image after nine iterations of demigration.

Migration using the decimated data results in CIGs such as the one shown in Figure 10b. The energy in the CIG that is outside the black dotted lines represents the migrated aliased events. This can clearly be concluded after comparing this CIG with the one in Figure 10a, which was migrated with the original nondecimated geometry.

To interpolate the decimated shot gathers to the same geometry of the original data, during gradient computation (equation 6) the data are acquired using the same geometry as the nondecimated data. First, we try to reconstruct the data using the CIGs without any modification. For obvious reasons, if we use the decimated data as a starting point for demigration, the residual would be zero and the objective function would have been minimized. So, here, similar to the first example, we start with a collection of zeroed traces and rely on the CIGs to reconstruct the data. The results of demigration after five iterations on a particular shot gather are shown in Figure 11b. The results show that demigration partially interpolates the decimated data, which now starts to resemble the nondecimated data, shown in Figure 11a. However, the

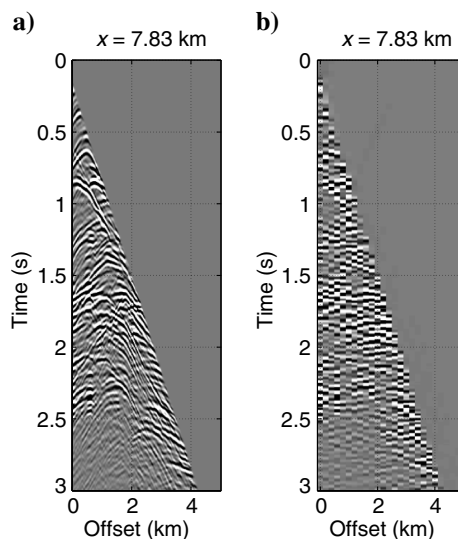


Figure 8. Original shot gathers; (a) nondecimated (0.025-m receiver interval) and (b) decimated by taking only every eighth trace (0.2-m receiver interval).

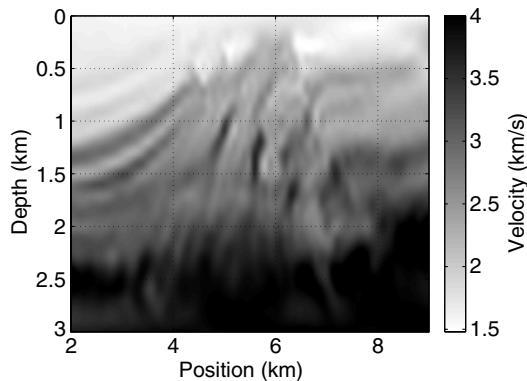


Figure 9. Marmousi migration velocity model used in example 2.

reconstructed data have artifacts in the form of collapsed diffractions. These imaged diffractions appear at the edges of the gaps in the decimated data.

To avoid these artifacts in the reconstructed data, we propose to mute the aliased energy in the CIGs before doing the demigration (Figure 10c). It is important that we are able to remove the aliasing artifacts without losing important reflection data information. When using a mute, the only way to achieve that goal is to use a migration velocity model that focuses the reflection energy in the region of the CIGs that is unaffected by the aliasing. This is the reason why we need to use a more accurate migration velocity model in this example than we used in the previous example. This allows us to choose a mute that removes most of the aliased energy while preserving the reflection information. The effect of aliasing is almost independent of the CIG position, which allows us to pick only one mute and use it for all CIGs. The chosen mute has a triangular shape and is defined by only three points; this is because the effect of aliasing is closer to zero lag at the shallow parts of the CIGs and almost linearly moves out toward higher lags with depth. The mute is applied with a short taper to prevent hard truncation, although the effect of having a hard mute has not been investigated. After muting, we demigrate the muted CIGs, acquiring the data at the original receiver geometry. The results of demigration of the muted CIGs after five iterations are shown in Figure 11c. The artifacts present in the case of demigration with the unprocessed CIGs are now greatly reduced, and the reconstructed shot gather compares more favorably with the original nondecimated shot gather shown in Figure 11a. Figure 11d shows the difference between the original nondecimated shot gather and the interpolated shot gather of Figure 11c. This figure shows that the reconstructed shot gather is approximately in phase with the original shot gather; however, given the approximate nature of this interpolation method, some difference is to be expected.

We observe that due to the smaller fold of the stack of the image constructed with the decimated data, the amplitudes of the reconstructed data will tend to converge to different values (about eight times smaller in this case) from those of the original data. Also, as mentioned, this procedure depends on having a migration velocity model that will focus the energy within the non-aliased part of the stack of the image constructed with the decimated data, that is, inside the black dotted lines indicated in Figure 10b. Otherwise, vital parts of the data may be muted together with the aliased energy. Despite these limitations, this type of reconstruction can find useful application in interpolating irregularly sampled aliased data, where most classical methods fail (Zwartjes and Sacchi, 2007).

It is also possible to use this procedure to interpolate across shot gathers. This can be achieved in exactly the same way as above, but by using reciprocity (Ikelle and Amundsen, 2005) and demigrating common receiver gathers, instead of common shot gathers.

### Example 3

We now present an application of the demigration method to free-surface-multiple attenuation. The migration velocity model is shown in Figure 12. We migrate the data using a grid cell

size of 0.0062 by 0.0062 km in the  $x$ - and  $z$ -directions. The maximum time used in modeling is 1.5 s. The time step size used is 1 ms, and the wavefields used for the imaging condition are sampled every 4 ms. We use monopole point sources with a 30-Hz Ricker wavelet as source functions. We use 81 horizontal half spatial lags for the imaging condition, which give a range between  $-0.25$  and  $0.25$  km for the half-offset vector. The migrated stacked image and CIGs are shown in Figure 13.

To remove the multiples, we explore a particular characteristic of the behavior of multiples in images migrated using the spatial lag extended crosscorrelation imaging condition. In these CIGs, free-surface multiples and primaries can be separated by noting that events requiring faster and slower velocities to be focused are shifted in opposite directions relative to the zero lag. This behavior

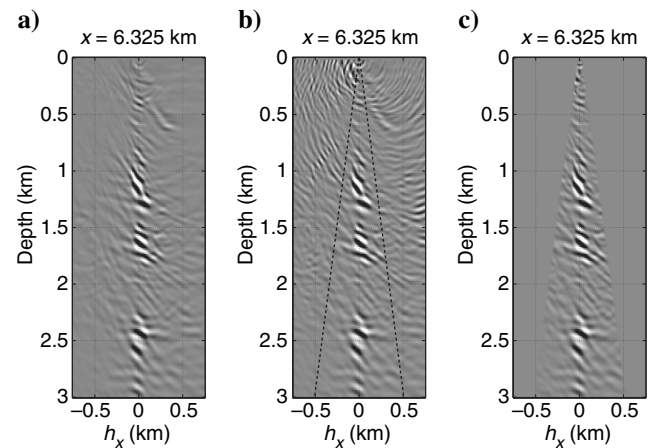


Figure 10. CIG at position 6.325 km migrated (a) with nondecimated data, (b) with decimated data, before mute, and (c) with decimated data, after mute to remove aliased events. The black dotted lines in (b) mark the position of the picked mute. The same mute is applied to all other CIGs. Note that after mute, the CIG migrated with the decimated data better approximates the CIG migrated with the full data.

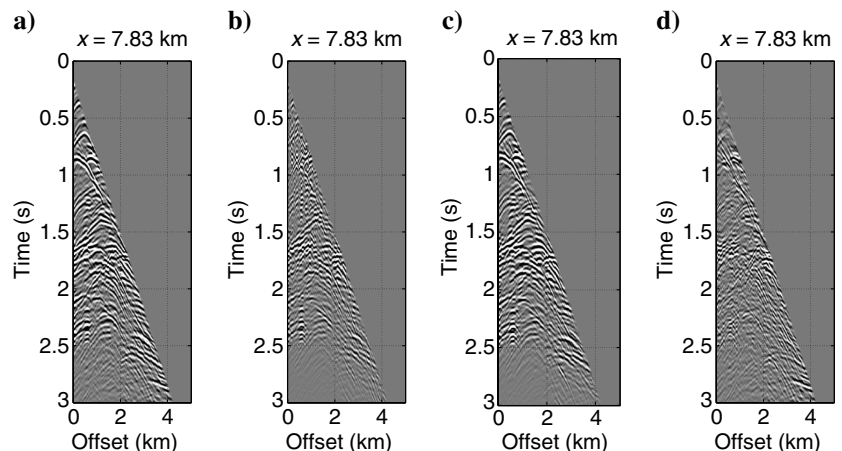


Figure 11. Shot gathers at position 7.83 km; (a) original, (b) reconstructed from the CIGs migrated with the decimated data without the mute to remove aliased energy, (c) reconstructed from the CIGs migrated with the decimated data with the mute to remove aliased energy, and (d) difference between shot gathers (a and c). Both reconstructed shot gathers correspond to the results after five iterations of demigration.

is first pointed out by [Mulder and van Leeuwen \(2008\)](#) and later explored by [Weibull and Arntsen \(2013\)](#) to attenuate multiples before automatic velocity analysis. The demultiple procedure consists of muting the multiple events in the CIGs and reconstructing the data using the demigration method presented in this paper.

Figure 14a shows one particular CIG at position 4 km, and Figure 14b shows the same CIG after amplitude equalization. The amplitude equalization consists of squaring the amplitudes of the CIGs and normalizing them at each depth with the maximum squared amplitude value for that depth. The amplitude equalization

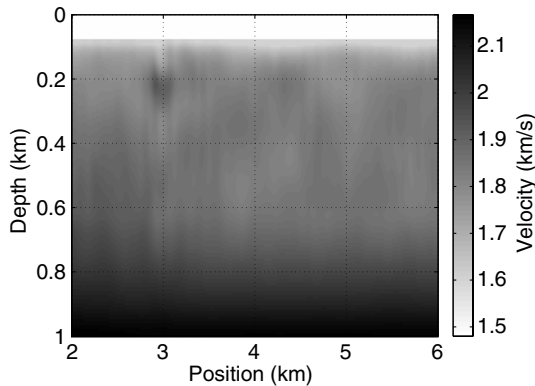


Figure 12. Migration velocity model for North Sea field data set.

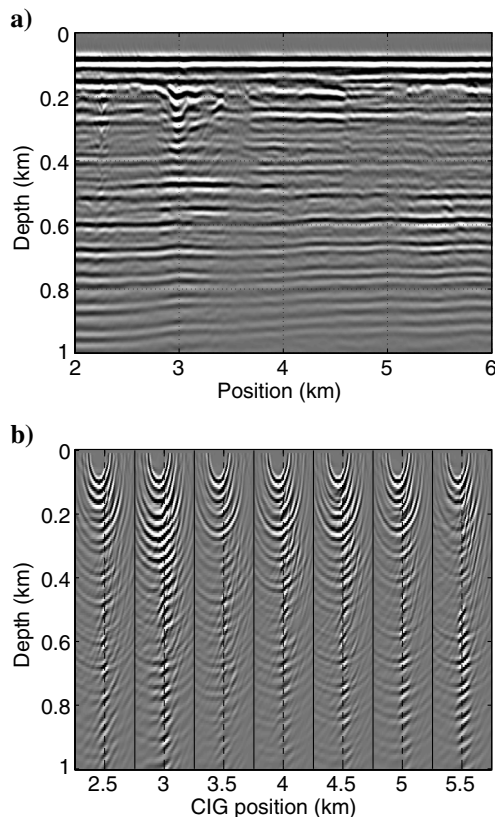


Figure 13. North Sea field data migrated; (a) zero-lag image and (b) CIGs at selected spatial positions. In the CIGs, the half-offsets range between  $-0.25$  and  $0.25$  km

is for visualization purposes because it helps in distinguishing between individual events in the CIG. This is useful for picking a mute to remove the free-surface-related multiple events in the CIGs, as we describe below. In Figure 14, the black dotted lines mark the position of the zero horizontal lag. Note that the events to the right of the black dotted lines represent events that require lower velocity for focusing. Here, we assume that the migration velocities are approximately accurate for focusing the primaries. Therefore, the events to the right of the strong events at the zero lag in the CIGs are interpreted as multiples and thus need to be muted.

Ideally, the mute needs to be picked exactly in between the primaries and the multiples as to preserve most of the primary energy and remove most of the multiple energy. Because our migration velocities are only approximately accurate, the primaries are not exactly lined up with the zero lag in all positions, and we need to apply a different mute to each CIG. To avoid picking a mute to every CIG, we manually pick mutes every  $0.62$  km (on every 100th CIG), and interpolate in between. Figure 14c shows the CIG at position 4 km after the mute is applied to it.

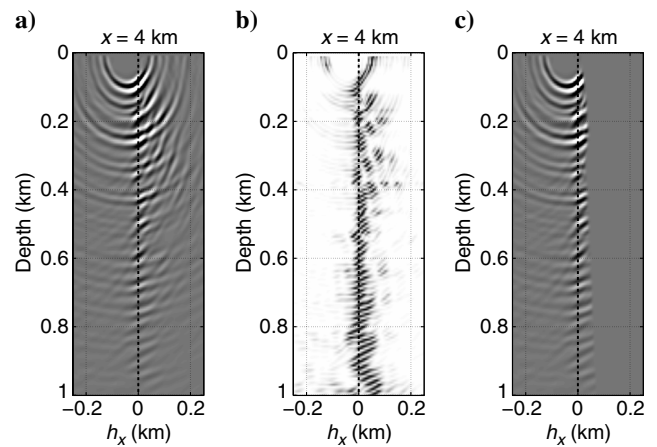


Figure 14. North Sea field data CIG at position 4 km; (a) original, (b) after amplitude equalization (see text for details), and (c) after mute to remove free-surface multiples.

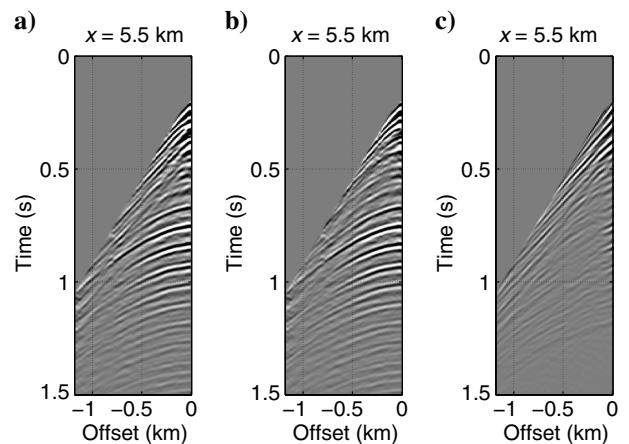


Figure 15. North Sea field data shot gathers at position 5.5 km; (a) original, (b) after 50 iterations of demigration of the muted CIGs, and (c) the difference between shot gathers (a) and (b).

After muting the CIGs, we run 50 iterations of demigration, using the original multiple-rich shot gathers as a starting point for the inversion. Figure 15a shows one of the original shot gathers that were used to generate the CIGs and also as a starting point for the inversion. Figure 15b shows the result of demigration of the muted CIGs on a particular shot gather at the same position. Finally, Figure 15c shows the difference between the original and demigrated shot gathers. As can be clearly seen, the free-surface-related multiple events that were muted in the CIGs are attenuated in the demigrated shot gather.

## CONCLUSION

We presented a method to reconstruct seismic reflection data from modified stacked CIGs constructed through RTM with an extended imaging condition. The method is based on least-squares inversion, and it is solved iteratively using a steepest-descent approach.

The numerical examples show that the extended imaging condition allows good reconstruction of the prestack seismic reflection data after only a few iterations. The presented method has many interesting applications, such as image-space multiple removal and data interpolation. In addition to this, because the method is based on RTM, it can be applied to process data acquired over complex geologic media.

## ACKNOWLEDGMENTS

We thank Ivan Vasconcelos, Clément Fleury, and four anonymous reviewers for constructive and appreciated criticism.

## REFERENCES

- Biondi, B., and G. Shan, 2002, Prestack imaging of overturned reflections by reverse time migration: 72nd Annual International Meeting, SEG, Expanded Abstracts, 1284–1287.
- Chauris, H., and M. Benjema, 2010, Seismic wave-equation demigration/migration: *Geophysics*, **75**, no. 3, S111–S119, doi: [10.1190/1.3380705](https://doi.org/10.1190/1.3380705).
- Claerbout, J. F., 1971, Toward a unified theory of reflector mapping: *Geophysics*, **36**, 467–481, doi: [10.1190/1.1440185](https://doi.org/10.1190/1.1440185).
- Claerbout, J. F., 1992, *Earth soundings analysis: Processing versus inversion*: Blackwell Scientific Publications, Inc.
- Guitton, A., B. Kaelin, and B. Biondi, 2007, Least-squares attenuation of reverse-time-migration artifacts: *Geophysics*, **72**, no. 1, S19–S23, doi: [10.1190/1.2399367](https://doi.org/10.1190/1.2399367).
- Ikelle, L. T., and L. Amundsen, 2005, *Introduction to petroleum seismology*: SEG.
- Jaramillo, H., and N. Bleistein, 1999, The link of Kirchhoff migration and demigration to Kirchhoff and Born modeling: *Geophysics*, **64**, 1793–1805, doi: [10.1190/1.1444685](https://doi.org/10.1190/1.1444685).
- Loewenthal, D., L. Lu, R. Roberson, and J. Sherwood, 1976, The wave equation applied to migration: *Geophysical Prospecting*, **24**, 380–399, doi: [10.1111/j.1365-2478.1976.tb00934.x](https://doi.org/10.1111/j.1365-2478.1976.tb00934.x).
- Miranda, F., 2006, Non-asymptotic seismic data reconstruction: 76th Annual International Meeting, SEG, Expanded Abstracts, 3016–3020.
- Mulder, W. A., and T. van Leeuwen, 2008, Automatic migration velocity analysis and multiples: 78th Annual International Meeting, SEG, Expanded Abstracts, 3128–3132.
- Nemeth, T., C. Wu, and G. T. Schuster, 1999, Least-squares migration incomplete reflection data: *Geophysics*, **64**, 208–221, doi: [10.1190/1.1444517](https://doi.org/10.1190/1.1444517).
- Nocedal, J., and S. J. Wright, 2000, *Numerical optimization*: Springer.
- Rickett, J. E., and P. C. Sava, 2002, Offset and angle-domain common image-point gathers for shot-profile migration: *Geophysics*, **67**, 883–889, doi: [10.1190/1.1484531](https://doi.org/10.1190/1.1484531).
- Santos, L., J. Schleicher, M. Tygel, and P. Hubral, 2000, Seismic modeling by demigration: *Geophysics*, **65**, 1281–1289, doi: [10.1190/1.1444819](https://doi.org/10.1190/1.1444819).
- Sava, P., and S. Fomel, 2006, Time-shift imaging condition in seismic migration: *Geophysics*, **71**, no. 6, S209–S217, doi: [10.1190/1.2338824](https://doi.org/10.1190/1.2338824).
- Sava, P., and I. Vasconcelos, 2011, Extended imaging conditions for wave-equation migration: *Geophysical Prospecting*, **59**, 35–55, doi: [10.1111/j.1365-2478.2010.00888.x](https://doi.org/10.1111/j.1365-2478.2010.00888.x).
- Symes, W. W., 2008, Migration velocity analysis and waveform inversion: *Geophysical Prospecting*, **56**, 765–790, doi: [10.1111/j.1365-2478.2008.00698.x](https://doi.org/10.1111/j.1365-2478.2008.00698.x).
- Versteeg, R. J., 1993, Sensitivity of prestack depth migration to the velocity model: *Geophysics*, **58**, 873–882, doi: [10.1190/1.1443471](https://doi.org/10.1190/1.1443471).
- Virieux, J., 1986, P-SV wave propagation in heterogeneous media; Velocity-stress finite-difference method: *Geophysics*, **51**, 889–901, doi: [10.1190/1.1442147](https://doi.org/10.1190/1.1442147).
- Weibull, W. W., and B. Arntsen, 2013, Automatic velocity analysis with reverse-time migration: *Geophysics*, **78**, no. 4, S179–S192, doi: [10.1190/geo2012-0064.1](https://doi.org/10.1190/geo2012-0064.1).
- Zhang, Y., and L. Duan, 2012, Predicting multiples using a reverse time demigration: 82nd Annual International Meeting, SEG, Expanded Abstracts, doi: [10.1190/segam2012-0520.1](https://doi.org/10.1190/segam2012-0520.1).
- Zwartjes, P., and M. Sacchi, 2007, Fourier reconstruction of nonuniformly sampled, aliased seismic data: *Geophysics*, **72**, no. 1, V21–V32, doi: [10.1190/1.2399442](https://doi.org/10.1190/1.2399442).